A New Code for Spectrometric Analysis for Environmental Radiological Surveillance on Monitors Focused on Gamma Radioactivity on Aerosols

Alfredo de Blas, *Member, IEEE*, Albert Riego, Roger Garcia, Carlos Tapia, Javier Dies, Juan Toral, Enric Batalla, and Pedro Diaz

***Abstract*—This paper presents a new code for the analysis of gamma spectra generated by an equipment for continuous measurement of gamma radioactivity in aerosols with paper filter. It is called pGamma and has been developed by the Nuclear Engineering Research Group at the Technical University of Catalonia - Barcelona Tech and by Raditel Serveis i Subministraments Tecnològics, Ltd. The code has been developed to identify the gamma emitters and to determine their activity concentration. It generates alarms depending on the activity of the emitters and elaborates reports. Therefore it includes a library with NORM and artificial emitters of interest. The code is being adapted to the monitors of the Environmental Radiological Surveillance Network of the local Catalan Government in Spain (Generalitat de Catalunya) and is used at three stations of the Network.**

***Index Terms*—Environmental radiation, gamma activity, gamma spectrometry, isotope identification.**

I. Introduction

THE use of monitors with spectrometric capability in environmental radiological surveillance networks provides additional information that complements the ambient dose equivalent $H^*(10)$. Based on this premise, our group (Nuclear Engineering Research Group) at the Technical University of Catalonia - Barcelona Tech and Raditel Serveis i Subministraments Tecnològics, Ltd. have developed an equipment for continuous measurement and identification of gamma radioactivity in aerosols with paper filter. Gamma spectrum analysis allows the identification and determination of activity concentration of radiation sources. Excellent commercial software is available for this purpose (among others, GammaVision form ORTEC and Genie2000 from CANBERRA). Nevertheless, it is generic software not intended for automatic analysis since each individual analysis must be conducted by a specialised technician. For this reason, our research group has developed a spectrometric analysis code specifically designed for the above equipment. This code is being used at stations with aerosol monitors on the Environmental Radiological Surveillance Network of the Generalitat de Catalunya (local Catalan Government), Spain[1]: Three monitors are currently fully operative: two in the surveillance station of the Ascó and Vandellòs Nuclear Power Plants (both in the province of Tarragona, Spain), and one in the Engineering School of Barcelona, Spain. Two new monitors will shortly be deployed in Roses (province of Girona) and in Puigcerdà (province of Barcelona). The code has been adapted for the analysis of gamma spectra generated by other monitors with spectrometric capability of the Network, i.e. river and direct air monitors. We are starting the tuning of these versions of the code on the monitors for river and direct air.

The code, called pGamma, discriminates spectrum information, identifies emitters appearing on the spectrum, determines activity concentration in $\mathrm{Bq/m^3}$ and generates alarms according to its calculated values. It has a normal operation mode and special operation mode for spectra obtained during energy calibration of the equipment. Additionally, another mode called investigation, is set when the variation in the total number of counts exceeds a certain level, or when a full energy peak is not identified.

The code input is an ASCII text file with the number of counts per channel of the spectrum and a header with information about measurement conditions: date and time of counting initiation and termination, live time, air flow, operation mode, the parameters of the energy calibration curve, etc. Fig. 1 is a general operation diagram of pGamma in normal operation mode.

The paper is organized as follows: Section II describes the treatment of the peaks in the spectrum. In Section III, efficiency calibration is presented. The determination procedure of activity concentration is shown in Section IV. Section V describes the identification of ^{131}I. In Section VI, the action levels are

Manuscript received May 27, 2015; revised October 12, 2015; accepted January 21, 2016.

A. de Blas, A. Riego, R. Garcia, C. Tapia, J. Dies, and P. Diaz are with the Nuclear Engineering Research Group, Department of Physics and Nuclear Engineering, Technical University of Catalonia, 08028 Barcelona, Spain (e-mail: alfredo.de.blas@upc.edu).

J. Toral is with Raditel Serveis, 43005 Tarragona, Spain (e-mail: raditelserveis@gmail.com).

E. Batalla is with the Radiological Activities Corrdination Service (SCAR) of the Generalitat de Catalunya, 08003 Barcelona, Spain (e-mail: ebatalla@gencat.cat).

Color versions of one or more of the figures in this paper are available online at http://ieeexplore.ieee.org.

Digital Object Identifier 10.1109/TNS.2016.2521388

[1]This network is integrated in the Spanish Nuclear Security Council network.

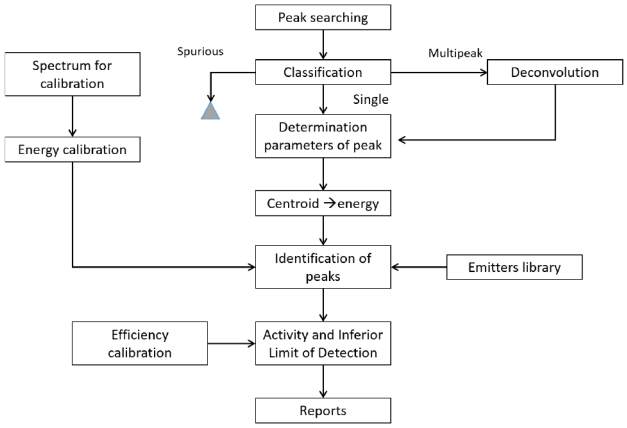

F1:1 Fig. 1. General diagram of pGamma.

presented. An Ascó station spectrum is analised in Section VII. Finally, conclusions are drawn in Section VIII.

II. Peak Treatment

The first step in the analysis of the spectrum is the treatment of the peaks: the searching of possible peaks on the spectrum and its identification.

A. Peak Search

Peak search and analysis is performed after the input spectrum is smoothed using the Savitzky-Golay method [1]. The smoothing algorithm allows the first, second and third derivatives of the spectrum to be obtained. The first derivative is used to determine the local maximums, which are subjected to a statistical test to discriminate real centrer of peaks (centroids) from spurious transitions. The nearest relative maximums of the first derivative at both sides of the centroid, indicate the channel of the peak boundaries. Using the second and the third derivate, single peaks are discriminated from multiplets. With the centroid and the boundaries of the peaks, the net area and the background are determined. The last step is the fitting of each peaks to a Gaussian curve. It allows the determination of the full width at half maximum (FWHM) and perform the chi-square test for further discrimination. With this information, pGamma generates a first list of possible peaks with their characteristics. The calculated parameters are centroid, lower and upper boundaries of the possible peak, full width at half maximum, gross area and net area.

B. Peak Identification

1) Energy Calibration: The use of energy calibration makes it possible to state the centroid, FWHM and limits of peaks in energy units instead of number of channels. The relationship between energy and adopted number of channel is:

$$E = a + bC + cC^2 \quad (1)$$

Where C is the channel and a, b and c are the parameters of the calibration curve. Energy calibration must be performed prior to installation of equipment in a station.

2) Peak Identification: Peaks can be identified using the library of gamma emitters of interest included in the code. This library has been created by us using information from [2]. For aerosol equipment, these emitters are the NORM radionuclides (^{238}U-^{222}Rn series, ^{232}Th-^{220}Rn series, ^{40}K and ^{7}Be) and artificial emitters from nuclear power plant discharges (e.g. radio-iodines, ^{137}Cs, ^{134}Cs and ^{132}Te) or industrial applications. Information about emitters includes energy and the emission probability of emitted gamma rays, empirical thresholds for NORM emitters to decide if pGamma must switch to investigation mode and derived concentration limits in the air.

The centroid energy of each peak is compared with the energy of gamma emitters. For similar values, the emitters are considered candidates for that peak and a list of candidates is generated. To identify a set of peaks with a radionuclide with multiple gamma emissions, the ratio between intensity of detected gammas and total intensity of the gammas of the emitter in the library is used. The relationship between the members of ^{238}U-^{222}Rn series and ^{232}Th-^{220}Rn series is considered too. pGamma cannot determine activity concentration of unidentified peaks.

III. Detection Efficiency Calibration

In order to determine activity concentration, the code needs information about the detection efficiency. Since the factors integrating the detection efficiency are very difficult to determine due to a complex geometry and a wide range of possible energies, efficiency calibration must be performed. First, the same geometry of the paper filter (source), detector and detection volume of the equipment during normal operation must be reproduced. This implies preparing a calibration source by shaping it into a disc with the same diameter of aerosols retained on the filter, and the same self-absorption (negligible) and gamma emitters of several energies in the range from 100 keV to 2000 keV. In consequence, the analytical determination of efficiency is cumbersome. The solution consists in using a calibration source with similar characteristics to the source to be measured and determining efficiency from experimental values. To ensure unbiased calibration, the calibration source should be identical to the radioactive samples in all aspects affecting detection [3]. If no calibration source is available or more points are required for adjusting the efficiency curve, Monte Carlo n-Particle (MCNP5, version 2.6.0) provide a further possibility for calculating the detector efficiency.

We used simulated ^{131}I and commercial ^{60}Co sources (Table I) with similar geometry and materials to those of the impregnated filter of the monitor. The simulated ^{131}I source is composed of two radioisotopes: ^{133}Ba and ^{137}Cs. The combination of both emitters generates a gamma energy spectrum whose full energy peaks have centroids and a relationship of areas very similar to the ^{131}I spectrum. The simulated ^{131}I source has the same area as the impregnated filter. The emitter material is deposited on a polymeric membrane with a stainless steel backing of 0.762 mm thickness and an 0.9 mg/cm^2 aluminized mylar window. Gamma absorption of the window and the backscattering on the back of the membrane are negligible. Therefore, it can be considered that the material and geometry

T1:1 TABLE I
T1:2 CHARACTERISTICS OF THE CALIBRATION SOURCES (REFERENCE FOR
T1:3 ACTIVITY: 01-JANUARY-2014)

(a)

Nuclides	^{137}Cs, ^{133}Ba
^{137}Cs Activity	0.4096 kBq
^{133}Ba Activity	4.222 kBq
^{131}I Activity	3.684 kBq
Manufacturer	Eckert & Ziegeler
Model	EAB-131(s)-PL
Source No.	K9-928

(b)

Activity	3.863 kBq
Manufacturer	Eckert & Ziegeler
Model	EAB-060-PL
Source No.	K9-925

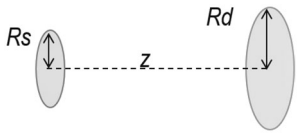

F2:1 Fig. 2. Geometry for equations (2) and (4).

T2:1 TABLE II
T2:2 EXPERIMENTAL DETECTION EFFICIENCY

Peak	E_i (keV)	N_i (cps)	$S_i(ph/s)$	ε_d
^{131}I sim	53.160	57.990	88.510	0.70319
^{131}I sim	276.390	40.801	296.150	0.14786
^{131}I sim	303.000	86.024	758.550	0.12170
^{131}I sim	356.010	184.860	2566.500	0.017730
^{131}I sim	661.500	19.830	385.100	0.05527
^{60}Co	1173.000	108.028	3573.290	0.03244
^{60}Co	1332.000	97.690	3579.020	0.02929

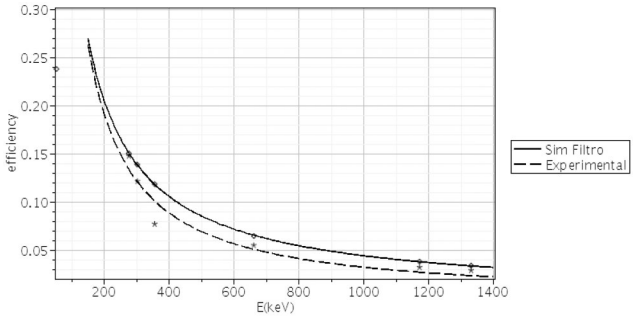

Fig. 3. Curve of efficiency. F3:1

of the source have the same behaviour as the impregnated paper filter. To simulate the detector response on the MCNP5 simulation we had used the FWHM obtained from the peaks on the spectra for the calibration sources (^{131}I and ^{60}Co) with the experimental setup. The function used is:

$$FWHM = 0.008 + 0.013 \cdot \sqrt{E + 0.593 \cdot E^2} \tag{2}$$

where E is the energy in MeV and the FWHM obtained is also in MeV.

Experimental efficiencies were obtained by analyzing the experimental spectra of ^{131}I and ^{60}Co by pGamma. Before the calculation of the efficiency, the net counts of the experimental peaks had to be compensated by a correction factor. The source capsule elevated the membrane where the radioactive material is deposited such that the membrane is slightly higher than the paper filter (about 0.283 cm). Assuming that both sources, the impregnated paper filter in normal operation and the calibration source, are discs and the detector window is a disc too (geometry on Fig. 2), we could determine the geometric factor in both cases using the following expansion in power series:

$$gf_i = \frac{1}{2}\left(1 - \frac{1}{R}\right) - \frac{3 \cdot \omega^2 \psi^2}{16 \cdot R^5} \cdot \left[1 - \frac{5\psi^2}{6 \cdot R^4} \cdot \left(1 - \frac{3 \cdot \omega^2}{4}\right) + \frac{35 \cdot \psi^4}{48 \cdot R^8}\left(1 - \frac{5 \cdot \omega^2}{2} + \frac{5 \cdot \omega^4}{8}\right) + \cdots\right] \tag{3}$$

the factors R, ψ and ω are determined as:

$$\psi = \frac{R_S}{z}; \omega = \frac{R_d}{z}; R = \sqrt{1 + \omega^2} \tag{4}$$

where R_S is the source radius, R_d is the detector radius, z is the distance between the source and the detector. Equation (4) can be applied either for the calibration source or the impregnated filter. Then the correction factor cf is:

$$cf = \frac{gf_{calibrationsoruce}}{gf_{filter}} \tag{5}$$

where gf is the geometric factor. With this method, the correction factor is 0.93680. By using seven MCNP5 code simulations, one for each energy, the mean correction factor is 0.93184. Efficiency ε_d for energy E_i is determined as:

$$\varepsilon_d = \frac{1}{cf} \cdot \frac{N_i}{S_i} \tag{6}$$

where N_i represents the net count rate of the full energy peak corresponding to the source gamma rays with energy E_i and S_i is the intensity of photons with energy E_i. Intensity is determined for the two components of the simulated ^{131}I: ^{137}Cs and ^{133}Ba, which are treated as two separate sources.

$$S_i = \nu_i \cdot A_i(0) e^{-T_t \cdot \lambda_i}; i = {}^{137}Cs, {}^{133}Ba \tag{7}$$

where ν_i is the emission probability of photons with energy E_i, $A_i(0)$ is the activity on the calibration date of the source, T_t is the time between the calibration date of the source and the day of the experiment and λ_i is the disintegration constant. With equations (6) and (7) we find the values of ε_d on Table II. A second efficiency curve, obtained from MCNP5, is compared with that obtained from experimental values, Fig. 3. As can be seen, the two curves are very close, with the exception of experimental efficiency for 380 keV. By fitting the experimental points without considering the 380 keV experimental value, efficiency is:

$$\varepsilon_d = \begin{cases} 0.43792 & 100keV \leq E \leq 200\text{keV} \\ 60.71703 \cdot E^{-1.07096} & E > 200\text{keV} \end{cases} \tag{8}$$

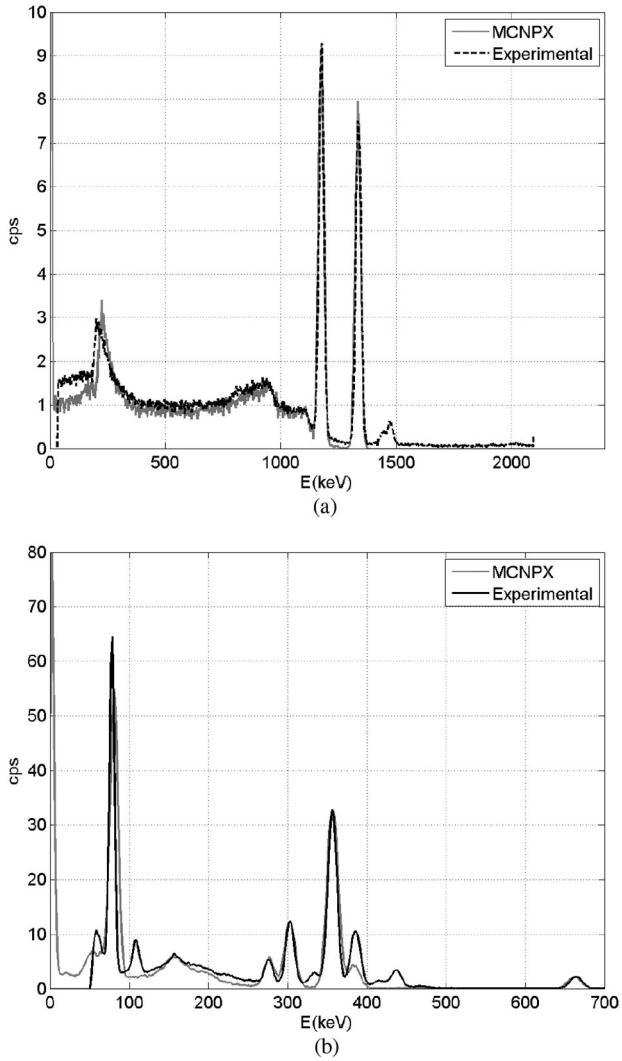

F4:1 Fig. 4. Comparison between simulated and experimental spectra. Experimental
F4:2 setup: $LaBr_3 2'' \times 2''$ scintillator and the DigiBASE compact instrumentation
F4:3 from ORTEC. The source is inside the volume of detection equipment for con-
F4:4 tinuous measurement and identification of gamma radioactivity in aerosols with
F4:5 paper filter. (a) Co-60 (b) Simulated I-131.

Since Monte Carlo methods were used to complement the experimental values to obtain the efficiency curve, the equipment simulation model must be benchmarked. In fact, without the geometry correction, Fig. 3 itself could be a validation of the Monte Carlo simulations. It is interesting to analyze and compare the experimental and Monte Carlo simulated spectra of the equipment with the calibration source instead of the paper filter. As the sources were very close to the front window of the detector, some true coincidence summing peaks appeared on the spectrum. These cannot be reproduced with a single MCNP5 simulation, but as we want to compare the procedure used to obtain the efficiency curve and these sum peaks are not required for the efficiency calculations, we will not simulate them. Fig. 4 compares simulated and experimental ^{60}Co and simulated source of ^{131}I spectra. The simulation reproduces perfectly the processes that not depend on the electronic instrumentation modules. As can be seen, backscattering peaks, Compton continuum, Compton valley and two full energy peaks appear. The differences between both spectra are due to the fact that background radiation is not simulated. Intrinsic radiation from the $LaBr_3$(Ce) scintillator, i.e. ^{138}La and ^{138}La plus X-rays peaks at 1468 keV, appears in the experimental spectrum. This component was not simulated, but is not relevant for efficiency calibration. Moreover, at low energies the simulated spectrum has fewer counts than the experimental one. This is because the Monte Carlo model does not simulate the background radiation components of cosmic rays or earth' s NORMs, resulting in fewer X-rays on the lead shielding (peak near 80 keV in the spectrum). In our model, only X-rays from absorption of the calibration source radiation are generated. Again, this is not important for efficiency calculation.

TABLE III T3:1
COMPARISON OF NET COUNTS OF PEAKS T3:2

	Net Counts ^{60}Co (cps)	
E (keV)	Experim.	MCNP
1173	107.95	122.13
1332	97.62	112.34

	Net Conts ^{131}I (cps)		Gross counts ^{131}I (cps)	
E (keV)	Experim.	MCNPX	Experim.	MCNP
60	24.11	8.60	57.99	65.19
80	189.18	303.36	260.91	380.45
276	21.02	17.61	40.80	44.48
303	63.31	73.27	86.02	104.65
356	184.86	249.07	231.13	291.88
661.5	19.83	22.51	22.32	22.79

Since the simulated ^{131}I has many peaks at low energies, the effect of sum peaks is more noticeable, at least in our energy range (0-2048 keV). Monte Carlo does not generate sum peaks, as can be seen in Fig. 4. For full energy peaks with little or no influence of sum peaks, simulation results are good. Table III compares the net areas of full energy peaks of simulated and experimental spectra. Peaks influenced by a sum peak are not used in efficiency calibration.

IV. DETERMINATION OF THE ACTIVITY CONCENTRATION

After identification of gamma emitters in the spectrum, the spectrometric analysis system determines their specific activity in the air $\tilde{A}_a$, expressed in Bq/m^3, according to the net area of the most efficient emitter of the isotope. However, the obtained spectrum corresponds to the number of counts caused by the radionuclide concentration on the filter, which is different from the radionuclide concentration in the air. Because the activity on the filter A_f is proportional to the number of captured atoms, a balance of activity can be performed in the same way as for concentration. The radionuclide concentration of an analysed emitter on the filter at a certain time depends on three factors: 1) **t**he number of captured atoms of this emitte**r**; 2) decays of the parent nuclei of this emitter, and 3) decays of this emitter.

Activity on the filter A_f is proportional to activity in the air $\tilde{A}_a$, air flow Q, and retention efficiency of the filter ε_f [4], [5]. Nevertheless, as activity on the filter implies a balance of matter on the filter, concentration of each radionuclide depends on its

position in the decay series. In the case of aerosol equipment, the radionuclides are belonging to the ^{238}U-^{222}Rn series, the ^{232}Th-^{220}Rn (chiefly ^{212}Pb, ^{212}Bi and ^{208}Tl) series or to none of the series. A slightly different statement is required for each case.

A. Radionuclides not Belonging to a Series

Most artificial emitters fall in this category. The balance of matter in this case is simply:

$$\frac{dA_f}{dt} = Q\varepsilon_f \tilde{A}_a(0) - \lambda_i A_f \tag{9}$$

Equation (9) can be solved by integration and as result the filter activity of the emitter analysed is:

$$A_f(t) = \frac{Q{\cdot}\varepsilon_f{\cdot}\tilde{A}_a}{\lambda}\int_0^T 1 - e^{-\lambda t}dt \tag{10}$$

Then, from Equation (10), the specific activity $\tilde{A}_a$ in the air for emitter i (expressed Bq/m^3) is:

$$\tilde{A}_a = \frac{\lambda_i N_i T}{Q\varepsilon_f\varepsilon_d\nu_i\int_0^T(1-e^{-\lambda_i t})dt} \tag{11}$$

Where λ_i is the decay constant for radionuclide i, N_i the net area (counts per second) of the full energy peak of the most probable gamma of radionuclide i, T the detection time (live time fo the Multiple Channel Analyzer), Q the average airflow, ε_f the filter efficiency, ε_d the detection efficiency for the most probable gamma of radionuclide i, and ν_i the emission probability of the most probable gamma of radionuclide i.

B. $^{238}U-^{222}Rn$ Series

The gamma emitters in the air of interest belonging to the decay series of ^{238}U are the descendents of ^{222}Rn:

$$^{222}\mathrm{Rn} \xrightarrow{\alpha} {}^{218}\mathrm{Po}(1) \xrightarrow{\alpha} {}^{214}\mathrm{Pb}(2) \xrightarrow{\beta} {}^{214}\mathrm{Bi}(3) \tag{12}$$

Numbers in parenthesis in the chain (12) represent the nomenclature used for the radionuclides in the following equations. These radionuclides are present on all countings because they come from the earth and surrounding buildings. Among them we can find some gamma emitters of certain importance, mainly ^{214}Pb and ^{214}Bi. The equations of balance of matter for chain (12) are:

$$\begin{aligned}
\frac{dA_{f1}}{dt} &= \tilde{A}_{a1}(0)Q\varepsilon_f - \lambda_1 A_{f1}\\
\frac{A_{f2}}{dt} &= \lambda_1 A_{f1} + \tilde{A}_{a2}(0)Q\varepsilon_f - \lambda_2 A_{f2}\\
\frac{dA_{f3}}{dt} &= \lambda_2 A_{f2} + \widetilde{A}_{a3}(0)Q\varepsilon_d - \lambda_3 A_{f3}
\end{aligned} \tag{13}$$

^{218}Po reaches its equilibrium at 95% in 13 minutes. By comparing the partial time of detection of 1 h and the total time of detection of 24 h, the hypothesis that ^{218}Po and ^{214}Pb are in equilibrium in the air can be supported.

$$\tilde{A}_{a1}(0) = \tilde{A}_{a2}(0) \tag{14}$$

By considering the equilibrium condition Eq. (14) and developing the balance equations Eq. (13), the specific activities of ^{214}Pb and ^{214}Bi can be determined **by**:

$$\tilde{A}_{a2}(0) = \frac{1}{2}\frac{N_2 T\lambda_2}{Q\nu_2\varepsilon_f\varepsilon_{d_2}\int_0^T(1-e^{-\lambda_2 t})dt} \tag{15}$$

The equation of balance of matter for chain 12 **is** (for simplicity we omit the explicit time dependences here):

$$\begin{aligned}
\tilde{A}_{a3}(0) = {} & \frac{\lambda_3 N_3 T}{Q\nu_3\varepsilon_f\varepsilon_{d_3}\int_0^T(1-e^{-\lambda_3 t})dt}\\
& - \frac{2\tilde{A}_{a2}(0)}{\int_0^T(1-e^{-\lambda_3 t})\,dt}\left[\int_0^T(1-e^{-\lambda_3 t})dt\right.\\
& \left. + \frac{\lambda_3}{\lambda_2-\lambda_3}\int_0^T\left(e^{-\lambda_2 t}-e^{-\lambda_3 t}\right)dt\right]
\end{aligned} \tag{16}$$

Emission probability ν_i, the net area of the full energy peak N_i and detection efficiency ε_i correspond to the most probable gamma of the analised radionuclide.

C. ^{232}Th- ^{220}Rn Series

As in the previous case, only the nuclides at the end of the chain are of interest in this series, i.e. from ^{220}Rn:

$$^{220}\mathrm{Rn} \xrightarrow{\alpha} {}^{216}\mathrm{Po}(1) \xrightarrow{\beta} {}^{212}\mathrm{Pb}(2) \xrightarrow{\beta} {}^{212}\mathrm{Bi}(3) \xrightarrow[34\,\%]{\beta} {}^{208}\mathrm{Tl}(4) \tag{17}$$

These radionuclides are always present in air aspiration, like in the previous series. Among them, ^{212}Pb, ^{212}Bi and ^{208}Tl are detected by the equipment. ^{212}Pb bifurcates to ^{208}Tl with 35.94% and to ^{212}Po with 64.06%, but ^{212}Po is not an important γ emitter. However, in the location areas of our monitoring stations there are fewer of those than of the ^{238}U-^{222}Rn series, and in typical spectra generated by the equipment only the presence of ^{212}Pb is detected. The balance of matter is similar to that of the previous series Eq. 13. The half-life of ^{216}Po is 0.15 s. Hence, it can be assumed that at the end of detection equilibrium exists between ^{216}Po and ^{212}Bi.

V. Analysis of ^{131}I

A. Identification and Minimum Detectable Activity (MDA)

Full energy peaks of ^{131}I gamma emitters are very close to some full energy peaks of ^{212}Pb, ^{214}Pb and ^{214}Bi. These natural emitters belong to the ^{222}Rn radon and ^{220}Rn thoron series, and are always present in the spectrum. Overlapping **o**f iodine gamma lines with other emmiters occurs between the 284.2 keV, 364.4 keV and 636.97 keV peaks of ^{131}I. The 722.89 keV peak does not overlap with those of natural emitters, but it has very low emission probability. Like the 80.18 keV of ^{131}I, that does not overlap with other peaks, but is outside the linear operating range of the scintillator. Therefore, to identify ^{131}I we can only use full energy peaks overlapped with natural emitter peaks, which are always present in the

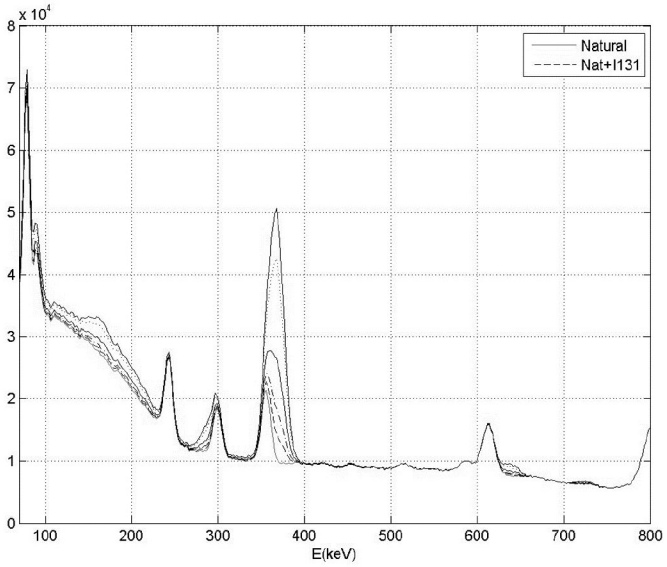

F5:1 Fig. 5. Spectra of ^{131}I. Obtained by a combination of experimental back-
F5:2 ground and simulations with the filter impregnated with ^{131}I. The different
F5:3 lines represents the spectra for different concentrations of ^{131}I.

spectrum. As a consequence, the minimum detectable activity of ^{131}I is greater than for other emitters.

Identification of ^{131}I was accomplished using several equipment simulations where the filter was impregnated with ^{131}I. These simulated spectra was combined with an experimental background spectrum. The resultant spectra is shown in Fig. 5 When the 364.4 keV peak is identified as ^{131}I instead of ^{214}Pb in the combined spectrum analised by pGamma, the activity of ^{131}I ranges between 0.4 Bq/m^3 and 0.8 Bq/m^3. The latter is its Minimum Detectable Activity (MDA). For comparison, ^{60}Co MDA is 0.02402 Bq/m^3 and ^{137}Cs MDA is 0.01662 Bq/m^3 (the air flow for the experimental background spectrum was 8.870m^3/h).

B. Determination of Specific Activity

The activity concentration of ^{131}I can be determined using the filter' s retention efficiency, which has already been studied by several authors ([4], [5]). It depends on the iodine species, particle size and air flow. The equipment for continuous measurement and identification of gamma radioactivity in aerosols for which this version of the pGamma code has been developed uses a GF 10 from Hahnemühle fiberglass paper filter. The fiberglass paper filter can only retain iodine particles. Their average size can be found in a number of works [6], [7]. Their diameter typically ranges between 0.2 μm and 0.5 μm. The air flow of the equipment in normal operation is 110m^3/h. In these conditions, the efficiency of the GF 10 filter for iodide can be considered as:

$$\varepsilon_f = \begin{cases} 99 - 0\% \text{(for particles)} \\ 0\% \text{(for all the other cases)} \end{cases} \quad (18)$$

However, the estimation of filter efficiency is not enough to determine the activity concentration of ^{131}I. Iodine can appear as a particle or gas in the form of elemental I or I^2, organic (chiefly methyl iodide CH^{3}I) or inorganic (hypoiodous HOI). The GF 10 filter does not capture all iodine species (actually, no filter does); it only retains particles. The only way to determine total activity concentration in the air is to know the concentration of iodine particles at the surveillance station, but this is impossible because of the special behavior of iodine transport in the atmosphere. The composition of iodine can be measured by gas chromatography [8], but this method is outside the equipment's concept. Several authors have made estimates from information collected during the Chernobyl or Fukushima accidents. For example, in [9] it was estimated that 50% of iodine is particles and the rest is gaseous. In his book [10], A. C. Chamberlain reports some particle-gas rate values, but they differ significantly from each other. Finally, the assumption in RASCAL 4.3 code [11], i.e. 33% of iodine particles, was considered for this work. We must bear in mind that the final purpose of the equipment is not to perform accurate measurements of air component concentration, but to provide information about gamma emitters in the air, such as the above estimates.

VI. Action Levels

Three action levels are provisionally considered[2]:

1) Investigation level.
2) Alert level, according to the concentration limit value in the air for public members (concentration giving by a dose 1 mSv/year).
3) Alarm level, according to twice the concentration limit value for the public.

The investigation level is initiated when:

1) The activity detected exceeds activity concentration thresholds for critical anthropogenic or natural isotopes stored in a library. For the former, the threshold is based on the recommendation of the 18 December 2003 Commission, (2004/2/EURATOM) DO L2/36 (6.1.2004). For NORM radionuclides, the threshold is based on station measurement values (e.g. $2 \cdot 10^{-2}$ Bq/m^3 for ^{131}I and $3 \cdot 10^{-2}$ Bq/m^3 for ^{137}Cs).
2) The analysis report contains one or more unidentified peaks.
3) The variation of the total number of counts on the detector during consecutive identical periods of time, defined as Relative Variation in the Number of Counts (RVC), exceeds an empirical value. This can be expressed as:

$$\frac{dC}{C} = \frac{C(t_2) - C(t_1)}{C(t_1)} \quad (19)$$

Where $C(t_1)$ and $C(t_2)$ are the number of counts on two consecutive identical periods of time. After a year of operation we propose a statistic analysis of the results and a revision of the investigation levels.

[2]Provided by the Spanish "Consejo de Seguridad Nuclear" (Nuclear Security Council)

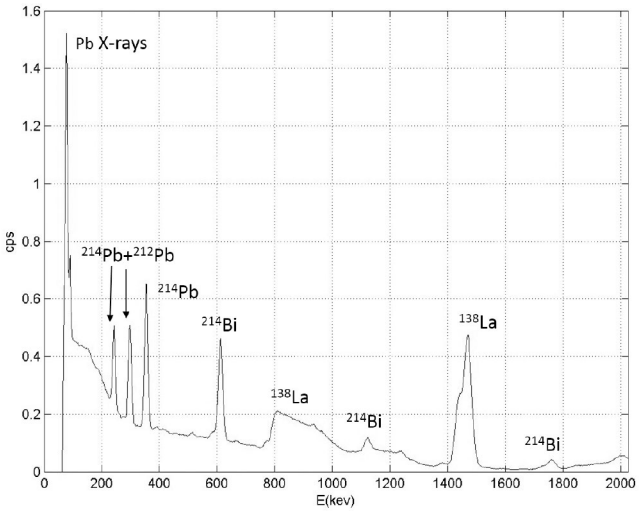

F6:1 Fig. 6. Spectrum analised, obtained with the equipment for continuous measurement and identification of gamma radioactivity in aerosols with paper filter
F6:2 ($2'' \times 2''$LaBr$_3$ scintillator with digiBASE form ORTEC).
F6:3

T4:1 TABLE IV
T4:2 DETECTABLE NORM GAMMA EMITTERS FROM AERSOLS [12]

Emitter	Series	Gammas emitted (keV)
^{214}Pb	^{238}U-^{222}Rn	242 (7.2 %), 295.22 (18.5%), 351.93 (35.6 %)
^{214}Bi	^{238}U-^{222}Rn	609.31 (45.49 %), 1120.29 (14.09 %), 1764.49 (15.28 %), 1847.42 (2 %) 2204.21 (4.9 %)
^{212}Pb	^{232}Th-^{220}Rn	238.63 (43.6 %), 300.09 (3.18 %)
^{212}Bi	^{232}Th-^{220}Rn	727.33 (6.74 %), 1620.74 (1.51 %)
^{208}Tl	^{232}Th-^{220}Rn	510.7 (6.29 %), 583.19 (30.6 %),2614.51 (35.85 %)

VII. ANALYSIS OF A SPECTRUM BY PGAMMA

This section presents a pGamma analysis example of a typical 24 h spectrum obtained at Ascó station on 10 January 2015. The average air flow was 8.35 Bq/m^3, there was no rainfall and the temperature ranged between $7°$C and $15°$C. The spectrum is shown in Fig. 6. Note that the peaks caused by NORM, i.e. detectable gamma emitters of the ^{238}U series and ^{212}Pb of the ^{232}Th series, appear combined with the intrinsic spectrum of the LaBr$_3$ detector. No anthropogenic emitters are observed in the air.

Considering the spectrum in Fig. 6, the components are: 1) Aerosols (mainly NORM) retained on the filter; 2) Cosmic particles and their interaction with elements on the detection zone and 3) Intrinsic spectrum of the detector. Table IV illustrates the detectable gamma peaks of the ^{238}U and ^{232}Th series. Fig. 7 shows the background spectrum (without air suction or aerosol retention) generated by the equipment. The cosmic component is only important at low energies. The level of intrinsic radiation from the detector is very significant in the range of interest, even higher than for the component resulting from aerosols retained on the filter. The radiation generated in the LaBr$_3$ crystal is mainly due to ^{138}La (Fig. 8). The most important peaks of the intrinsic spectrum of the LaBr$_3$ scintillation detector are: 1) between (0-300) keV β continuous; 2) between (700-1100) keV β continuous plus gammas of 789 keV; 3) between (1400-1500) keV gammas of 1436 keV and a sum peak of gammas of 1436 keV and X-rays of 32 keV.

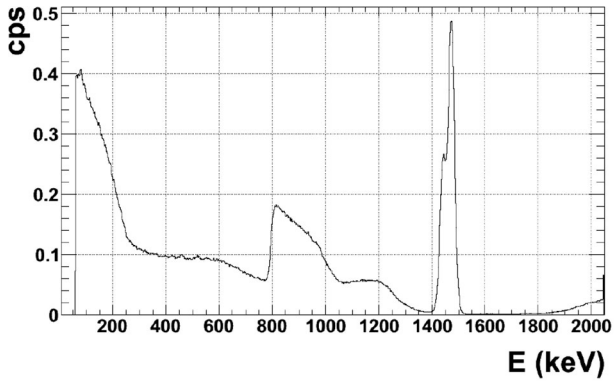

Fig. 7. Background spectrum of the equipment of the measurement of gamma radiation on aerosols by paper filter. F7:1 F7:2

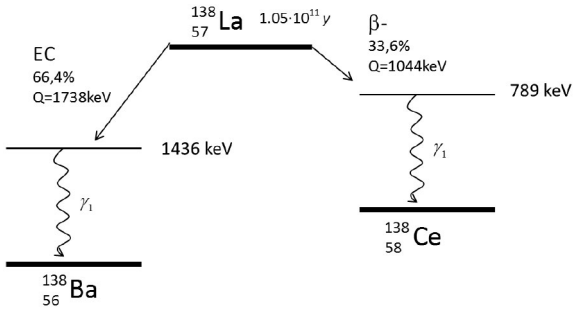

Fig. 8. Decay scheme for ^{138}La [13]. F8:1

Fig. 9 shows the pGamma report of the analised spectrum. The report has four parts: 1) overall parameters of the spectrum; 2) specific activity of identified isotopes (first column for activity, second for error and third for the minimum detectable activity); 3) identified peaks; and 4) unidentified peaks.

Following the list of expected peaks (Table IV), the code identified: 1) The most probable ^{214}Pb peaks; 2) The most probable ^{214}Bi peaks; 3) One ^{212}Pb peak; and 4) The 789 keV and of 1436 keV γ peaks and the combination of the γ of 1436 keV with the X-ray of 32 keV of the intrinsic spectrum of the LaBr$_3$ crystal. ^{212}Bi does not appear in the list of identified peaks because its gamma rays have a very low emission probability and its full energy peaks are not significant enough. ^{208}Tl has no identified peaks. From ^{208}Tl, the 510.7 keV peak is very close to the annihilation peak and is too small to be distinguished by a scintillator, the same is true of the 583.19 keV peak. This one is important but very close to the 609.31 keV peak of ^{214}Bi, which is a very significant one, and therefore the overlapping peak is assigned to ^{214}Bi. The 2614.51 keV peak is out of the operating range of the equipment. It must be remembered that, with the resolution of scintillators, the 242 keV and 295.22 keV peaks of ^{214}Pb coincide with the ^{212}Pb peaks. Finally, the peak 6 at 514.1 keV is the annihilation peak.

```
[1]
11640368
10179770
[2]
pb212 SerieTh232Rn220 3.15e-001 3.56e-003 6.98e-003 1
bi214 SerieU238Rn222 1.42e+001 8.05e-002 2.88e-001 7 10 11
12 13 17 18
pb214 SerieU238Rn222 1.49e+001 7.23e-002 1.47e-001 2 3
[3]
pb212 1 121.1 241.7 241.8 4.4 115 133 14.4 135857.7
SerieTh232Rn220
bi214 7 307.0 611.0 609.6 9.6 286 326 20.9 302812.7
SerieU238Rn222
bi214 10 467.6 932.4 936.5 5.4 464 479 18.4 5440.6
SerieU238Rn222
bi214 11 561.5 1121.2 1120.2 9.5 542 574 26.7 44514.1
SerieU238Rn222
bi214 12 618.1 1235.2 1238.1 6.3 612 667 23.1 8134.9
SerieU238Rn222
bi214 13 690.1 1380.9 1375.5 7.1 676 695 19.7 4868.6
SerieU238Rn222
bi214 17 876.3 1759.3 1753.0 17.6 846 894 33.7 51719.2
SerieU238Rn222
bi214 18 921.8 1852.1 1841.1 9.9 902 927 30.1 4166.6
SerieU238Rn222
pb214 2 148.9 296.7 296.9 4.8 142 158 17.3 178632.9
SerieU238Rn222
pb214 3 177.6 353.5 353.4 5.5 168 186 14.1 304242.5
SerieU238Rn222
aniq 6 257.8 512.9 514.1 5.3 252 266 17.0 7653.3 Pic
d'aniquilació
la138 9 405.2 807.1 818.3 19.8 391 438 52.7 172130.3
Intrinsec
la138 14 733.3 1468.4 1468.6 7.8 723 780 21.9 229245.5
Intrinsec
[4]
```

F9:1 Fig. 9. Report with the analysis of pGamma.

VIII. Conclusions

The pGamma code is an automatic spectrometric analysis system for environmental radiation monitoring equipment with spectrometric capability. The version presented in this paper was specifically designed for our equipment of continuous measurement and identification of gamma radioactivity in aerosols with paper filter. Nevertheless, the code is perfectly adaptable to other equipment of the environmental radiological surveillance network of the local Catalan Government. The code identifies gamma emitters in the energy spectrum and determines their specific activity. If an emitter is not identified or activity concentration of any identified emitter exceeds an empirical threshold, an alarm is generated.

References

[1] A. Savitzky and M. Golay, "Smoothing and differentiation of data by simplified least squares procedures," *Anal. Chem.*, vol. 36, pp. 1627–1639, 1964.

[2] E. Browne and R. Firestone, *Table of Radioactive Isotopes*, S. Shirley, Eds. New York, NY, USA: Wiley, 1986.

[3] S. Organizations, Multi-Agency Radiological Laboratory Analytical Protocols Manual (MARLAP). Cap 15 Quantification of Radionuclides. NUREG-1576 / EPA 402-B-04-001A / NTIS PB2004-105421, *United States Environmental Protection Agency et. al.*, Jul. 2004, http://www.epa.gov/radiation/marlap/manual.html

[4] W. John and G. Reischl, "Measurements of the filtration efficiencies of selected filter types," *Atmospher. Environ.*, vol. 12, pp. 2015–2019, 1978.

[5] E. Kitto and D. Anderson, "Correspondence. the use of whatman-41 filters for particle collection," *Atmospher. Environ.*, vol. 22, no. 11, pp. 2629–2630, 1988.

[6] Y. Miyamoto, K. Yasuda, and M. Magara, "Size distribution of radioactive particles collected at tokai, japan 6 days after the nuclear accident," *J. Environ. Radioact.*, vol. 132, pp. 1–7, 2014.

[7] E. Bondietti, J. Brantley, and C. Rangarajan, "Size distributions and growth of natural and chernobyl-derived submicron aerosols in tennessee," *J. Environ. Radioact.*, vol. 6, pp. 99–120, 1988.

[8] M. Naritomi, Y. Yoshida, and S. Fukuda, "Method for improving the collecting performance of iodine samplers under high relative humidity," *J. Nucl. Sci. Technol.*, vol. 10, no. 5, pp. 292–300, 1973.

[9] S. MacMullin, G. Giovanetti, M. Green, R. Henning, R. Holmes, K. Vorren, and J. Wilkerson, "Measurement of airborne fission products in Chapel Hill, NC, USA from the Fukushima Daiichi reactor accident," *J. Environ. Radioact.*, vol. 112, pp. 165–170, 2012.

[10] A. Chamberlain, *Radioactive Aerosols*, 1st Cambridge, U.K.: Cambridge Univ. Press, 1991.

[11] J. Ramsdell Jr., "Rascal 4.3. dispersion and deposition models," *Proc. 18th Annu. George Mason Univ. Conf. Atmospheric Transport and Dispersion Modelling*, 2014.

[12] G. Gilmore, *Practical Gamma-Ray Spectrometry*, Hoboken, NJ, USA: Wiley, 2008, http://books.google.es/books?id=mNHvAAAAMAAJ

[13] *Scintillation products, Tech. note, Brillance Scintillators Performance Summary,*, Saint Gobain Crystals Tech. Rep., 2009.

A New Code for Spectrometric Analysis for Environmental Radiological Surveillance on Monitors Focused on Gamma Radioactivity on Aerosols

Alfredo de Blas, *Member, IEEE*, Albert Riego, Roger Garcia, Carlos Tapia, Javier Dies, Juan Toral, Enric Batalla, and Pedro Diaz

***Abstract*—This paper presents a new code for the analysis of gamma spectra generated by an equipment for continuous measurement of gamma radioactivity in aerosols with paper filter. It is called pGamma and has been developed by the Nuclear Engineering Research Group at the Technical University of Catalonia - Barcelona Tech and by Raditel Serveis i Subministraments Tecnològics, Ltd. The code has been developed to identify the gamma emitters and to determine their activity concentration. It generates alarms depending on the activity of the emitters and elaborates reports. Therefore it includes a library with NORM and artificial emitters of interest. The code is being adapted to the monitors of the Environmental Radiological Surveillance Network of the local Catalan Government in Spain (Generalitat de Catalunya) and is used at three stations of the Network.**

***Index Terms*—Environmental radiation, gamma activity, gamma spectrometry, isotope identification.**

I. Introduction

THE use of monitors with spectrometric capability in environmental radiological surveillance networks provides additional information that complements the ambient dose equivalent $H^*(10)$. Based on this premise, our group (Nuclear Engineering Research Group) at the Technical University of Catalonia - Barcelona Tech and Raditel Serveis i Subministraments Tecnològics, Ltd. have developed an equipment for continuous measurement and identification of gamma radioactivity in aerosols with paper filter. Gamma spectrum analysis allows the identification and determination of activity concentration of radiation sources. Excellent commercial software is available for this purpose (among others, GammaVision form ORTEC and Genie2000 from CANBERRA). Nevertheless, it is generic software not intended for automatic analysis since each individual analysis must be conducted by a specialised technician. For this reason, our research group has developed a spectrometric analysis code specifically designed for the above equipment. This code is being used at stations with aerosol monitors on the Environmental Radiological Surveillance Network of the Generalitat de Catalunya (local Catalan Government), Spain[1]: Three monitors are currently fully operative: two in the surveillance station of the Ascó and Vandellòs Nuclear Power Plants (both in the province of Tarragona, Spain), and one in the Engineering School of Barcelona, Spain. Two new monitors will shortly be deployed in Roses (province of Girona) and in Puigcerdà (province of Barcelona). The code has been adapted for the analysis of gamma spectra generated by other monitors with spectrometric capability of the Network, i.e. river and direct air monitors. We are starting the tuning of these versions of the code on the monitors for river and direct air.

The code, called pGamma, discriminates spectrum information, identifies emitters appearing on the spectrum, determines activity concentration in $\mathrm{Bq/m^3}$ and generates alarms according to its calculated values. It has a normal operation mode and special operation mode for spectra obtained during energy calibration of the equipment. Additionally, another mode called investigation, is set when the variation in the total number of counts exceeds a certain level, or when a full energy peak is not identified.

The code input is an ASCII text file with the number of counts per channel of the spectrum and a header with information about measurement conditions: date and time of counting initiation and termination, live time, air flow, operation mode, the parameters of the energy calibration curve, etc. Fig. 1 is a general operation diagram of pGamma in normal operation mode.

The paper is organized as follows: Section II describes the treatment of the peaks in the spectrum. In Section III, efficiency calibration is presented. The determination procedure of activity concentration is shown in Section IV. Section V describes the identification of ^{131}I. In Section VI, the action levels are

Manuscript received May 27, 2015; revised October 12, 2015; accepted January 21, 2016.

A. de Blas, A. Riego, R. Garcia, C. Tapia, J. Dies, and P. Diaz are with the Nuclear Engineering Research Group, Department of Physics and Nuclear Engineering, Technical University of Catalonia, 08028 Barcelona, Spain (e-mail: alfredo.de.blas@upc.edu).

J. Toral is with Raditel Serveis, 43005 Tarragona, Spain (e-mail: raditelserveis@gmail.com).

E. Batalla is with the Radiological Activities Corrdination Service (SCAR) of the Generalitat de Catalunya, 08003 Barcelona, Spain (e-mail: ebatalla@gencat.cat).

Color versions of one or more of the figures in this paper are available online at http://ieeexplore.ieee.org.

Digital Object Identifier 10.1109/TNS.2016.2521388

[1]This network is integrated in the Spanish Nuclear Security Council network.

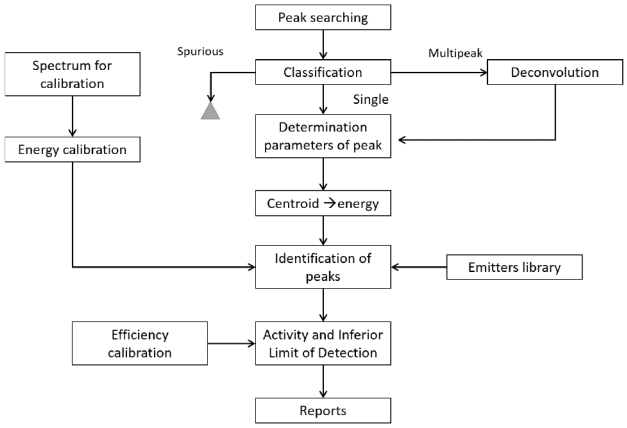

F1:1 Fig. 1. General diagram of pGamma.

presented. An Ascó station spectrum is analised in Section VII. Finally, conclusions are drawn in Section VIII.

II. Peak Treatment

The first step in the analysis of the spectrum is the treatment of the peaks: the searching of possible peaks on the spectrum and its identification.

A. Peak Search

Peak search and analysis is performed after the input spectrum is smoothed using the Savitzky-Golay method [1]. The smoothing algorithm allows the first, second and third derivatives of the spectrum to be obtained. The first derivative is used to determine the local maximums, which are subjected to a statistical test to discriminate real centrer of peaks (centroids) from spurious transitions. The nearest relative maximums of the first derivative at both sides of the centroid, indicate the channel of the peak boundaries. Using the second and the third derivate, single peaks are discriminated from multiplets. With the centroid and the boundaries of the peaks, the net area and the background are determined. The last step is the fitting of each peaks to a Gaussian curve. It allows the determination of the full width at half maximum (FWHM) and perform the chi-square test for further discrimination. With this information, pGamma generates a first list of possible peaks with their characteristics. The calculated parameters are centroid, lower and upper boundaries of the possible peak, full width at half maximum, gross area and net area.

B. Peak Identification

1) Energy Calibration: The use of energy calibration makes it possible to state the centroid, FWHM and limits of peaks in energy units instead of number of channels. The relationship between energy and adopted number of channel is:

$$E = a + bC + cC^2 \quad (1)$$

Where C is the channel and a, b and c are the parameters of the calibration curve. Energy calibration must be performed prior to installation of equipment in a station.

2) Peak Identification: Peaks can be identified using the library of gamma emitters of interest included in the code. This library has been created by us using information from [2]. For aerosol equipment, these emitters are the NORM radionuclides (^{238}U-^{222}Rn series, ^{232}Th-^{220}Rn series, ^{40}K and ^{7}Be) and artificial emitters from nuclear power plant discharges (e.g. radio-iodines, ^{137}Cs, ^{134}Cs and ^{132}Te) or industrial applications. Information about emitters includes energy and the emission probability of emitted gamma rays, empirical thresholds for NORM emitters to decide if pGamma must switch to investigation mode and derived concentration limits in the air.

The centroid energy of each peak is compared with the energy of gamma emitters. For similar values, the emitters are considered candidates for that peak and a list of candidates is generated. To identify a set of peaks with a radionuclide with multiple gamma emissions, the ratio between intensity of detected gammas and total intensity of the gammas of the emitter in the library is used. The relationship between the members of ^{238}U-^{222}Rn series and ^{232}Th-^{220}Rn series is considered too. pGamma cannot determine activity concentration of unidentified peaks.

III. Detection Efficiency Calibration

In order to determine activity concentration, the code needs information about the detection efficiency. Since the factors integrating the detection efficiency are very difficult to determine due to a complex geometry and a wide range of possible energies, efficiency calibration must be performed. First, the same geometry of the paper filter (source), detector and detection volume of the equipment during normal operation must be reproduced. This implies preparing a calibration source by shaping it into a disc with the same diameter of aerosols retained on the filter, and the same self-absorption (negligible) and gamma emitters of several energies in the range from 100 keV to 2000 keV. In consequence, the analytical determination of efficiency is cumbersome. The solution consists in using a calibration source with similar characteristics to the source to be measured and determining efficiency from experimental values. To ensure unbiased calibration, the calibration source should be identical to the radioactive samples in all aspects affecting detection [3]. If no calibration source is available or more points are required for adjusting the efficiency curve, Monte Carlo n-Particle (MCNP5, version 2.6.0) provide a further possibility for calculating the detector efficiency.

We used simulated ^{131}I and commercial ^{60}Co sources (Table I) with similar geometry and materials to those of the impregnated filter of the monitor. The simulated ^{131}I source is composed of two radioisotopes: ^{133}Ba and ^{137}Cs. The combination of both emitters generates a gamma energy spectrum whose full energy peaks have centroids and a relationship of areas very similar to the ^{131}I spectrum. The simulated ^{131}I source has the same area as the impregnated filter. The emitter material is deposited on a polymeric membrane with a stainless steel backing of 0.762 mm thickness and an 0.9 mg/cm^2 aluminized mylar window. Gamma absorption of the window and the backscattering on the back of the membrane are negligible. Therefore, it can be considered that the material and geometry

T1:1 TABLE I
T1:2 CHARACTERISTICS OF THE CALIBRATION SOURCES (REFERENCE FOR
T1:3 ACTIVITY: 01-JANUARY-2014)

(a)

Nuclides	^{137}Cs, ^{133}Ba
^{137}Cs Activity	0.4096 kBq
^{133}Ba Activity	4.222 kBq
^{131}I Activity	3.684 kBq
Manufacturer	Eckert & Ziegeler
Model	EAB-131(s)-PL
Source No.	K9-928

(b)

Activity	3.863 kBq
Manufacturer	Eckert & Ziegeler
Model	EAB-060-PL
Source No.	K9-925

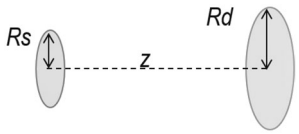

F2:1 Fig. 2. Geometry for equations (2) and (4).

of the source have the same behaviour as the impregnated paper filter. To simulate the detector response on the MCNP5 simulation we had used the FWHM obtained from the peaks on the spectra for the calibration sources (^{131}I and ^{60}Co) with the experimental setup. The function used is:

$$FWHM = 0.008 + 0.013 \cdot \sqrt{E + 0.593 \cdot E^2} \qquad (2)$$

where E is the energy in MeV and the FWHM obtained is also in MeV.

Experimental efficiencies were obtained by analyzing the experimental spectra of ^{131}I and ^{60}Co by pGamma. Before the calculation of the efficiency, the net counts of the experimental peaks had to be compensated by a correction factor. The source capsule elevated the membrane where the radioactive material is deposited such that the membrane is slightly higher than the paper filter (about 0.283 cm). Assuming that both sources, the impregnated paper filter in normal operation and the calibration source, are discs and the detector window is a disc too (geometry on Fig. 2), we could determine the geometric factor in both cases using the following expansion in power series:

$$gf_i = \frac{1}{2}\left(1 - \frac{1}{R}\right) - \frac{3 \cdot \omega^2 \psi^2}{16 \cdot R^5} \cdot \left[1 - \frac{5\psi^2}{6 \cdot R^4} \cdot \left(1 - \frac{3 \cdot \omega^2}{4}\right) + \frac{35 \cdot \psi^4}{48 \cdot R^8}\left(1 - \frac{5 \cdot \omega^2}{2} + \frac{5 \cdot \omega^4}{8}\right) + \cdots\right] \qquad (3)$$

the factors R, ψ and ω are determined as:

$$\psi = \frac{R_S}{z}; \omega = \frac{R_d}{z}; R = \sqrt{1 + \omega^2} \qquad (4)$$

where R_S is the source radius, R_d is the detector radius, z is the distance between the source and the detector. Equation (4) can

T2:1 TABLE II
T2:2 EXPERIMENTAL DETECTION EFFICIENCY

Peak	E_i (keV)	N_i (cps)	$S_i(ph/s)$	ε_d
^{131}I sim	53.160	57.990	88.510	0.70319
^{131}I sim	276.390	40.801	296.150	0.14786
^{131}I sim	303.000	86.024	758.550	0.12170
^{131}I sim	356.010	184.860	2566.500	0.017730
^{131}I sim	661.500	19.830	385.100	0.05527
^{60}Co	1173.000	108.028	3573.290	0.03244
^{60}Co	1332.000	97.690	3579.020	0.02929

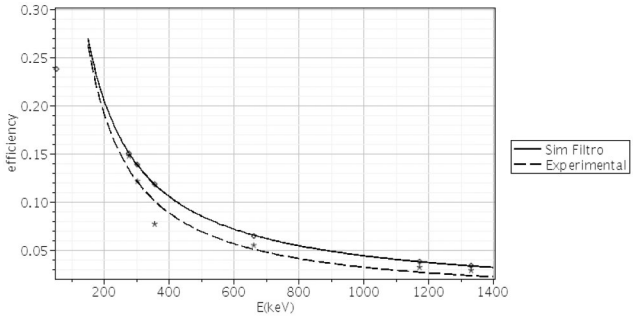

Fig. 3. Curve of efficiency. F3:1

be applied either for the calibration source or the impregnated filter. Then the correction factor cf is:

$$cf = \frac{gf_{calibrationsoruce}}{gf_{filter}} \qquad (5)$$

where gf is the geometric factor. With this method, the correction factor is 0.93680. By using seven MCNP5 code simulations, one for each energy, the mean correction factor is 0.93184. Efficiency ε_d for energy E_i is determined as:

$$\varepsilon_d = \frac{1}{cf} \cdot \frac{N_i}{S_i} \qquad (6)$$

where N_i represents the net count rate of the full energy peak corresponding to the source gamma rays with energy E_i and S_i is the intensity of photons with energy E_i. Intensity is determined for the two components of the simulated ^{131}I: ^{137}Cs and ^{133}Ba, which are treated as two separate sources.

$$S_i = \nu_i \cdot A_i(0) e^{-T_t \cdot \lambda_i}; i = {}^{137}Cs, {}^{133}Ba \qquad (7)$$

where ν_i is the emission probability of photons with energy E_i, $A_i(0)$ is the activity on the calibration date of the source, T_t is the time between the calibration date of the source and the day of the experiment and λ_i is the disintegration constant. With equations (6) and (7) we find the values of ε_d on Table II. A second efficiency curve, obtained from MCNP5, is compared with that obtained from experimental values, Fig. 3. As can be seen, the two curves are very close, with the exception of experimental efficiency for 380 keV. By fitting the experimental points without considering the 380 keV experimental value, efficiency is:

$$\varepsilon_d = \begin{cases} 0.43792 & 100keV \leq E \leq 200\text{keV} \\ 60.71703 \cdot E^{-1.07096} & E > 200\text{keV} \end{cases} \qquad (8)$$

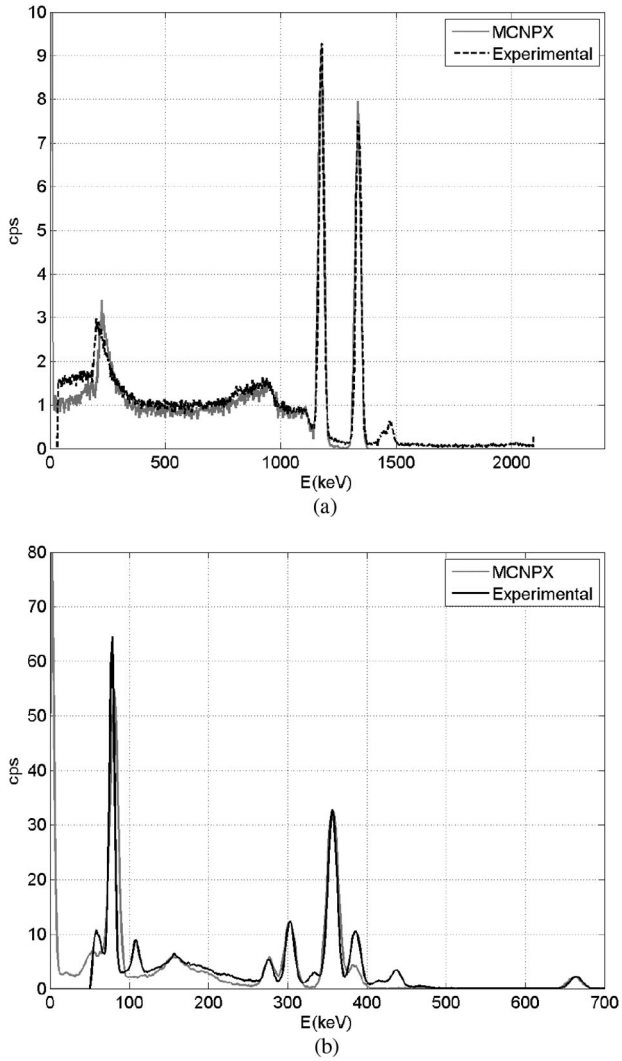

F4:1 Fig. 4. Comparison between simulated and experimental spectra. Experimental
F4:2 setup: $LaBr_3 2'' \times 2''$ scintillator and the DigiBASE compact instrumentation
F4:3 from ORTEC. The source is inside the volume of detection equipment for con-
F4:4 tinuous measurement and identification of gamma radioactivity in aerosols with
F4:5 paper filter. (a) Co-60 (b) Simulated I-131.

Since Monte Carlo methods were used to complement the experimental values to obtain the efficiency curve, the equipment simulation model must be benchmarked. In fact, without the geometry correction, Fig. 3 itself could be a validation of the Monte Carlo simulations. It is interesting to analyze and compare the experimental and Monte Carlo simulated spectra of the equipment with the calibration source instead of the paper filter. As the sources were very close to the front window of the detector, some true coincidence summing peaks appeared on the spectrum. These cannot be reproduced with a single MCNP5 simulation, but as we want to compare the procedure used to obtain the efficiency curve and these sum peaks are not required for the efficiency calculations, we will not simulate them. Fig. 4 compares simulated and experimental ^{60}Co and simulated source of ^{131}I spectra. The simulation reproduces perfectly the processes that not depend on the electronic instrumentation modules. As can be seen, backscattering peaks, Compton continuum, Compton valley and two full energy peaks appear. The differences between both spectra are due to the fact that background radiation is not simulated. Intrinsic radiation from the $LaBr_3$(Ce) scintillator, i.e. ^{138}La and ^{138}La plus X-rays peaks at 1468 keV, appears in the experimental spectrum. This component was not simulated, but is not relevant for efficiency calibration. Moreover, at low energies the simulated spectrum has fewer counts than the experimental one. This is because the Monte Carlo model does not simulate the background radiation components of cosmic rays or earth' s NORMs, resulting in fewer X-rays on the lead shielding (peak near 80 keV in the spectrum). In our model, only X-rays from absorption of the calibration source radiation are generated. Again, this is not important for efficiency calculation.

TABLE III T3:1
COMPARISON OF NET COUNTS OF PEAKS T3:2

	Net Counts ^{60}Co (cps)	
E (keV)	Experim.	MCNP
1173	107.95	122.13
1332	97.62	112.34

	Net Conts ^{131}I (cps)		Gross counts ^{131}I (cps)	
E (keV)	Experim.	MCNPX	Experim.	MCNP
60	24.11	8.60	57.99	65.19
80	189.18	303.36	260.91	380.45
276	21.02	17.61	40.80	44.48
303	63.31	73.27	86.02	104.65
356	184.86	249.07	231.13	291.88
661.5	19.83	22.51	22.32	22.79

Since the simulated ^{131}I has many peaks at low energies, the effect of sum peaks is more noticeable, at least in our energy range (0-2048 keV). Monte Carlo does not generate sum peaks, as can be seen in Fig. 4. For full energy peaks with little or no influence of sum peaks, simulation results are good. Table III compares the net areas of full energy peaks of simulated and experimental spectra. Peaks influenced by a sum peak are not used in efficiency calibration.

IV. DETERMINATION OF THE ACTIVITY CONCENTRATION

After identification of gamma emitters in the spectrum, the spectrometric analysis system determines their specific activity in the air $\tilde{A}_a$, expressed in $\mathrm{Bq/m^3}$, according to the net area of the most efficient emitter of the isotope. However, the obtained spectrum corresponds to the number of counts caused by the radionuclide concentration on the filter, which is different from the radionuclide concentration in the air. Because the activity on the filter A_f is proportional to the number of captured atoms, a balance of activity can be performed in the same way as for concentration. The radionuclide concentration of an analysed emitter on the filter at a certain time depends on three factors: 1) **t**he number of captured atoms of this emitte**r**; 2) decays of the parent nuclei of this emitter, and 3) decays of this emitter.

Activity on the filter A_f is proportional to activity in the air $\tilde{A}_a$, air flow Q, and retention efficiency of the filter ε_f [4], [5]. Nevertheless, as activity on the filter implies a balance of matter on the filter, concentration of each radionuclide depends on its

position in the decay series. In the case of aerosol equipment, the radionuclides are belonging to the ^{238}U-^{222}Rn series, the ^{232}Th-^{220}Rn (chiefly ^{212}Pb, ^{212}Bi and ^{208}Tl) series or to none of the series. A slightly different statement is required for each case.

A. Radionuclides not Belonging to a Series

Most artificial emitters fall in this category. The balance of matter in this case is simply:

$$\frac{dA_f}{dt} = Q\varepsilon_f \tilde{A}_a(0) - \lambda_i A_f \tag{9}$$

Equation (9) can be solved by integration and as result the filter activity of the emitter analysed is:

$$A_f(t) = \frac{Q{\cdot}\varepsilon_f{\cdot}\tilde{A}_a}{\lambda}\int_0^T 1 - e^{-\lambda t}dt \tag{10}$$

Then, from Equation (10), the specific activity $\tilde{A}_a$ in the air for emitter i (expressed Bq/m^3) is:

$$\tilde{A}_a = \frac{\lambda_i N_i T}{Q\varepsilon_f\varepsilon_d\nu_i\int_0^T(1-e^{-\lambda_i t})dt} \tag{11}$$

Where λ_i is the decay constant for radionuclide i, N_i the net area (counts per second) of the full energy peak of the most probable gamma of radionuclide i, T the detection time (live time fo the Multiple Channel Analyzer), Q the average airflow, ε_f the filter efficiency, ε_d the detection efficiency for the most probable gamma of radionuclide i, and ν_i the emission probability of the most probable gamma of radionuclide i.

B. $^{238}U-^{222}Rn$ Series

The gamma emitters in the air of interest belonging to the decay series of ^{238}U are the descendents of ^{222}Rn:

$$^{222}\mathrm{Rn} \xrightarrow{\alpha} {}^{218}\mathrm{Po}(1) \xrightarrow{\alpha} {}^{214}\mathrm{Pb}(2) \xrightarrow{\beta} {}^{214}\mathrm{Bi}(3) \tag{12}$$

Numbers in parenthesis in the chain (12) represent the nomenclature used for the radionuclides in the following equations. These radionuclides are present on all countings because they come from the earth and surrounding buildings. Among them we can find some gamma emitters of certain importance, mainly ^{214}Pb and ^{214}Bi. The equations of balance of matter for chain (12) are:

$$\begin{aligned}
\frac{dA_{f1}}{dt} &= \tilde{A}_{a1}(0)Q\varepsilon_f - \lambda_1 A_{f1}\\
\frac{A_{f2}}{dt} &= \lambda_1 A_{f1} + \tilde{A}_{a2}(0)Q\varepsilon_f - \lambda_2 A_{f2}\\
\frac{dA_{f3}}{dt} &= \lambda_2 A_{f2} + \widetilde{A}_{a3}(0)Q\varepsilon_d - \lambda_3 A_{f3}
\end{aligned} \tag{13}$$

^{218}Po reaches its equilibrium at 95% in 13 minutes. By comparing the partial time of detection of 1 h and the total time of detection of 24 h, the hypothesis that ^{218}Po and ^{214}Pb are in equilibrium in the air can be supported.

$$\tilde{A}_{a1}(0) = \tilde{A}_{a2}(0) \tag{14}$$

By considering the equilibrium condition Eq. (14) and developing the balance equations Eq. (13), the specific activities of ^{214}Pb and ^{214}Bi can be determined **by**:

$$\tilde{A}_{a2}(0) = \frac{1}{2}\frac{N_2 T\lambda_2}{Q\nu_2\varepsilon_f\varepsilon_{d_2}\int_0^T(1-e^{-\lambda_2 t})dt} \tag{15}$$

The equation of balance of matter for chain 12 **is** (for simplicity we omit the explicit time dependences here):

$$\begin{aligned}
\tilde{A}_{a3}(0) = {} & \frac{\lambda_3 N_3 T}{Q\nu_3\varepsilon_f\varepsilon_{d_3}\int_0^T(1-e^{-\lambda_3 t})dt}\\
& - \frac{2\tilde{A}_{a2}(0)}{\int_0^T(1-e^{-\lambda_3 t})\,dt}\left[\int_0^T(1-e^{-\lambda_3 t})dt\right.\\
& \left. + \frac{\lambda_3}{\lambda_2-\lambda_3}\int_0^T\left(e^{-\lambda_2 t}-e^{-\lambda_3 t}\right)dt\right]
\end{aligned} \tag{16}$$

Emission probability ν_i, the net area of the full energy peak N_i and detection efficiency ε_i correspond to the most probable gamma of the analised radionuclide.

C. ^{232}Th- ^{220}Rn Series

As in the previous case, only the nuclides at the end of the chain are of interest in this series, i.e. from ^{220}Rn:

$$^{220}\mathrm{Rn} \xrightarrow{\alpha} {}^{216}\mathrm{Po}(1) \xrightarrow{\beta} {}^{212}\mathrm{Pb}(2) \xrightarrow{\beta} {}^{212}\mathrm{Bi}(3) \xrightarrow[34\,\%]{\beta} {}^{208}\mathrm{Tl}(4) \tag{17}$$

These radionuclides are always present in air aspiration, like in the previous series. Among them, ^{212}Pb, ^{212}Bi and ^{208}Tl are detected by the equipment. ^{212}Pb bifurcates to ^{208}Tl with 35.94% and to ^{212}Po with 64.06%, but ^{212}Po is not an important γ emitter. However, in the location areas of our monitoring stations there are fewer of those than of the ^{238}U-^{222}Rn series, and in typical spectra generated by the equipment only the presence of ^{212}Pb is detected. The balance of matter is similar to that of the previous series Eq. 13. The half-life of ^{216}Po is 0.15 s. Hence, it can be assumed that at the end of detection equilibrium exists between ^{216}Po and ^{212}Bi.

V. Analysis of ^{131}I

A. Identification and Minimum Detectable Activity (MDA)

Full energy peaks of ^{131}I gamma emitters are very close to some full energy peaks of ^{212}Pb, ^{214}Pb and ^{214}Bi. These natural emitters belong to the ^{222}Rn radon and ^{220}Rn thoron series, and are always present in the spectrum. Overlapping **o**f iodine gamma lines with other emmiters occurs between the 284.2 keV, 364.4 keV and 636.97 keV peaks of ^{131}I. The 722.89 keV peak does not overlap with those of natural emitters, but it has very low emission probability. Like the 80.18 keV of ^{131}I, that does not overlap with other peaks, but is outside the linear operating range of the scintillator. Therefore, to identify ^{131}I we can only use full energy peaks overlapped with natural emitter peaks, which are always present in the

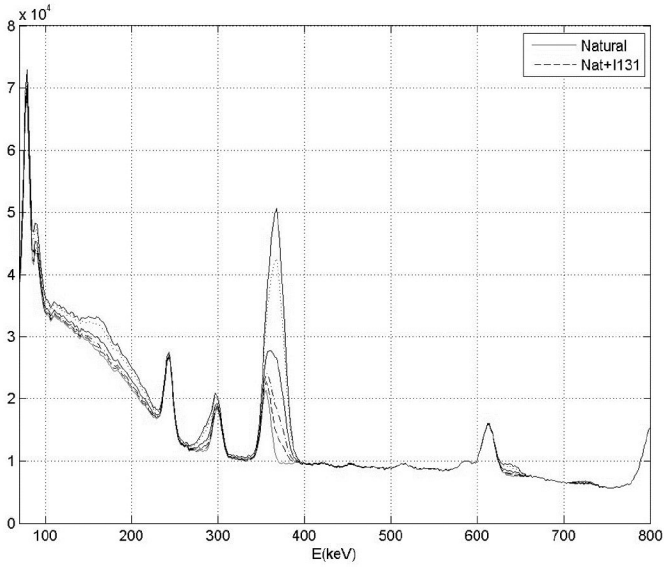

F5:1 Fig. 5. Spectra of ^{131}I. Obtained by a combination of experimental back-
F5:2 ground and simulations with the filter impregnated with ^{131}I. The different
F5:3 lines represents the spectra for different concentrations of ^{131}I.

spectrum. As a consequence, the minimum detectable activity of ^{131}I is greater than for other emitters.

Identification of ^{131}I was accomplished using several equipment simulations where the filter was impregnated with ^{131}I. These simulated spectra was combined with an experimental background spectrum. The resultant spectra is shown in Fig. 5 When the 364.4 keV peak is identified as ^{131}I instead of ^{214}Pb in the combined spectrum analised by pGamma, the activity of ^{131}I ranges between 0.4 Bq/m^3 and 0.8 Bq/m^3. The latter is its Minimum Detectable Activity (MDA). For comparison, ^{60}Co MDA is 0.02402 Bq/m^3 and ^{137}Cs MDA is 0.01662 Bq/m^3 (the air flow for the experimental background spectrum was 8.870m^3/h).

B. Determination of Specific Activity

The activity concentration of ^{131}I can be determined using the filter' s retention efficiency, which has already been studied by several authors ([4], [5]). It depends on the iodine species, particle size and air flow. The equipment for continuous measurement and identification of gamma radioactivity in aerosols for which this version of the pGamma code has been developed uses a GF 10 from Hahnemühle fiberglass paper filter. The fiberglass paper filter can only retain iodine particles. Their average size can be found in a number of works [6], [7]. Their diameter typically ranges between 0.2 μm and 0.5 μm. The air flow of the equipment in normal operation is 110m^3/h. In these conditions, the efficiency of the GF 10 filter for iodide can be considered as:

$$\varepsilon_f = \begin{cases} 99 - 0\% \text{(for particles)} \\ 0\% \text{(for all the other cases)} \end{cases} \quad (18)$$

However, the estimation of filter efficiency is not enough to determine the activity concentration of ^{131}I. Iodine can appear as a particle or gas in the form of elemental I or I^2, organic (chiefly methyl iodide CH^{3}I) or inorganic (hypoiodous HOI). The GF 10 filter does not capture all iodine species (actually, no filter does); it only retains particles. The only way to determine total activity concentration in the air is to know the concentration of iodine particles at the surveillance station, but this is impossible because of the special behavior of iodine transport in the atmosphere. The composition of iodine can be measured by gas chromatography [8], but this method is outside the equipment's concept. Several authors have made estimates from information collected during the Chernobyl or Fukushima accidents. For example, in [9] it was estimated that 50% of iodine is particles and the rest is gaseous. In his book [10], A. C. Chamberlain reports some particle-gas rate values, but they differ significantly from each other. Finally, the assumption in RASCAL 4.3 code [11], i.e. 33% of iodine particles, was considered for this work. We must bear in mind that the final purpose of the equipment is not to perform accurate measurements of air component concentration, but to provide information about gamma emitters in the air, such as the above estimates.

VI. Action Levels

Three action levels are provisionally considered[2]:

1) Investigation level.
2) Alert level, according to the concentration limit value in the air for public members (concentration giving by a dose 1 mSv/year).
3) Alarm level, according to twice the concentration limit value for the public.

The investigation level is initiated when:

1) The activity detected exceeds activity concentration thresholds for critical anthropogenic or natural isotopes stored in a library. For the former, the threshold is based on the recommendation of the 18 December 2003 Commission, (2004/2/EURATOM) DO L2/36 (6.1.2004). For NORM radionuclides, the threshold is based on station measurement values (e.g. $2 \cdot 10^{-2}$ Bq/m^3 for ^{131}I and $3 \cdot 10^{-2}$ Bq/m^3 for ^{137}Cs).
2) The analysis report contains one or more unidentified peaks.
3) The variation of the total number of counts on the detector during consecutive identical periods of time, defined as Relative Variation in the Number of Counts (RVC), exceeds an empirical value. This can be expressed as:

$$\frac{dC}{C} = \frac{C(t_2) - C(t_1)}{C(t_1)} \quad (19)$$

Where $C(t_1)$ and $C(t_2)$ are the number of counts on two consecutive identical periods of time. After a year of operation we propose a statistic analysis of the results and a revision of the investigation levels.

[2]Provided by the Spanish "Consejo de Seguridad Nuclear" (Nuclear Security Council)

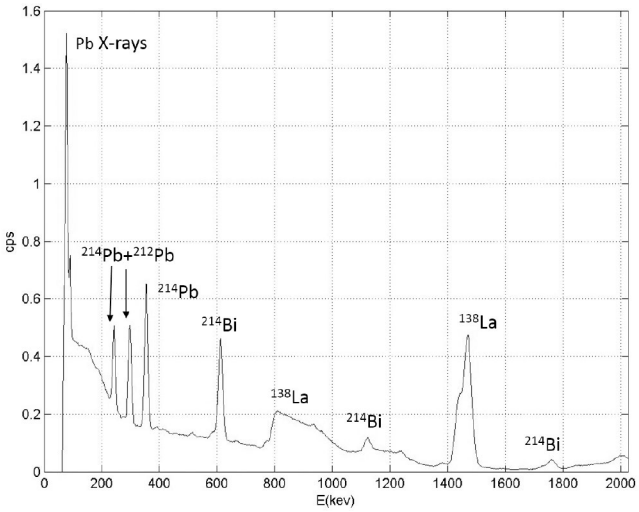

F6:1 Fig. 6. Spectrum analised, obtained with the equipment for continuous mea-
F6:2 surement and identification of gamma radioactivity in aerosols with paper filter
F6:3 ($2'' \times 2''$LaBr$_3$ scintillator with digiBASE form ORTEC).

T4:1 TABLE IV
T4:2 DETECTABLE NORM GAMMA EMITTERS FROM AERSOLS [12]

Emitter	Series	Gammas emitted (keV)
^{214}Pb	^{238}U-^{222}Rn	242 (7.2 %), 295.22 (18.5%), 351.93 (35.6 %)
^{214}Bi	^{238}U-^{222}Rn	609.31 (45.49 %), 1120.29 (14.09 %), 1764.49 (15.28 %), 1847.42 (2 %) 2204.21 (4.9 %)
^{212}Pb	^{232}Th-^{220}Rn	238.63 (43.6 %), 300.09 (3.18 %)
^{212}Bi	^{232}Th-^{220}Rn	727.33 (6.74 %), 1620.74 (1.51 %)
^{208}Tl	^{232}Th-^{220}Rn	510.7 (6.29 %), 583.19 (30.6 %),2614.51 (35.85 %)

VII. ANALYSIS OF A SPECTRUM BY PGAMMA

This section presents a pGamma analysis example of a typical 24 h spectrum obtained at Ascó station on 10 January 2015. The average air flow was 8.35 Bq/m^3, there was no rainfall and the temperature ranged between $7°$C and $15°$C. The spectrum is shown in Fig. 6. Note that the peaks caused by NORM, i.e. detectable gamma emitters of the ^{238}U series and ^{212}Pb of the ^{232}Th series, appear combined with the intrinsic spectrum of the LaBr$_3$ detector. No anthropogenic emitters are observed in the air.

Considering the spectrum in Fig. 6, the components are: 1) Aerosols (mainly NORM) retained on the filter; 2) Cosmic particles and their interaction with elements on the detection zone and 3) Intrinsic spectrum of the detector. Table IV illustrates the detectable gamma peaks of the ^{238}U and ^{232}Th series. Fig. 7 shows the background spectrum (without air suction or aerosol retention) generated by the equipment. The cosmic component is only important at low energies. The level of intrinsic radiation from the detector is very significant in the range of interest, even higher than for the component resulting from aerosols retained on the filter. The radiation generated in the LaBr$_3$ crystal is mainly due to ^{138}La (Fig. 8). The most important peaks of the intrinsic spectrum of the LaBr$_3$ scintillation detector are: 1) between (0-300) keV β continuous; 2) between (700-1100) keV β continuous plus gammas of 789 keV; 3) between (1400-1500) keV gammas of 1436 keV and a sum peak of gammas of 1436 keV and X-rays of 32 keV.

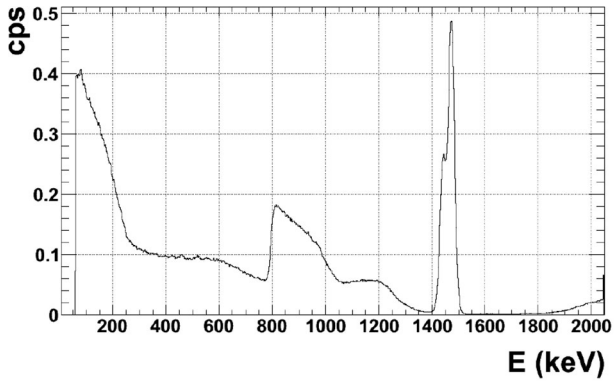

Fig. 7. Background spectrum of the equipment of the measurement of gamma radiation on aerosols by paper filter. F7:1 F7:2

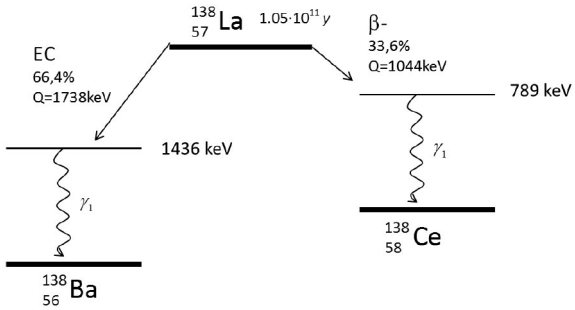

Fig. 8. Decay scheme for ^{138}La [13]. F8:1

Fig. 9 shows the pGamma report of the analised spectrum. The report has four parts: 1) overall parameters of the spectrum; 2) specific activity of identified isotopes (first column for activity, second for error and third for the minimum detectable activity); 3) identified peaks; and 4) unidentified peaks.

Following the list of expected peaks (Table IV), the code identified: 1) The most probable ^{214}Pb peaks; 2) The most probable ^{214}Bi peaks; 3) One ^{212}Pb peak; and 4) The 789 keV and of 1436 keV γ peaks and the combination of the γ of 1436 keV with the X-ray of 32 keV of the intrinsic spectrum of the LaBr$_3$ crystal. ^{212}Bi does not appear in the list of identified peaks because its gamma rays have a very low emission probability and its full energy peaks are not significant enough. ^{208}Tl has no identified peaks. From ^{208}Tl, the 510.7 keV peak is very close to the annihilation peak and is too small to be distinguished by a scintillator, the same is true of the 583.19 keV peak. This one is important but very close to the 609.31 keV peak of ^{214}Bi, which is a very significant one, and therefore the overlapping peak is assigned to ^{214}Bi. The 2614.51 keV peak is out of the operating range of the equipment. It must be remembered that, with the resolution of scintillators, the 242 keV and 295.22 keV peaks of ^{214}Pb coincide with the ^{212}Pb peaks. Finally, the peak 6 at 514.1 keV is the annihilation peak.

```
[1]
11640368
10179770
[2]
pb212 SerieTh232Rn220 3.15e-001 3.56e-003 6.98e-003 1
bi214 SerieU238Rn222 1.42e+001 8.05e-002 2.88e-001 7 10 11
12 13 17 18
pb214 SerieU238Rn222 1.49e+001 7.23e-002 1.47e-001 2 3
[3]
pb212 1 121.1 241.7 241.8 4.4 115 133 14.4 135857.7
SerieTh232Rn220
bi214 7 307.0 611.0 609.6 9.6 286 326 20.9 302812.7
SerieU238Rn222
bi214 10 467.6 932.4 936.5 5.4 464 479 18.4 5440.6
SerieU238Rn222
bi214 11 561.5 1121.2 1120.2 9.5 542 574 26.7 44514.1
SerieU238Rn222
bi214 12 618.1 1235.2 1238.1 6.3 612 667 23.1 8134.9
SerieU238Rn222
bi214 13 690.1 1380.9 1375.5 7.1 676 695 19.7 4868.6
SerieU238Rn222
bi214 17 876.3 1759.3 1753.0 17.6 846 894 33.7 51719.2
SerieU238Rn222
bi214 18 921.8 1852.1 1841.1 9.9 902 927 30.1 4166.6
SerieU238Rn222
pb214 2 148.9 296.7 296.9 4.8 142 158 17.3 178632.9
SerieU238Rn222
pb214 3 177.6 353.5 353.4 5.5 168 186 14.1 304242.5
SerieU238Rn222
aniq 6 257.8 512.9 514.1 5.3 252 266 17.0 7653.3 Pic
d'aniquilació
la138 9 405.2 807.1 818.3 19.8 391 438 52.7 172130.3
Intrinsec
la138 14 733.3 1468.4 1468.6 7.8 723 780 21.9 229245.5
Intrinsec
[4]
```

F9:1 Fig. 9. Report with the analysis of pGamma.

VIII. Conclusions

The pGamma code is an automatic spectrometric analysis system for environmental radiation monitoring equipment with spectrometric capability. The version presented in this paper was specifically designed for our equipment of continuous measurement and identification of gamma radioactivity in aerosols with paper filter. Nevertheless, the code is perfectly adaptable to other equipment of the environmental radiological surveillance network of the local Catalan Government. The code identifies gamma emitters in the energy spectrum and determines their specific activity. If an emitter is not identified or activity concentration of any identified emitter exceeds an empirical threshold, an alarm is generated.

References

[1] A. Savitzky and M. Golay, "Smoothing and differentiation of data by simplified least squares procedures," *Anal. Chem.*, vol. 36, pp. 1627–1639, 1964.

[2] E. Browne and R. Firestone, *Table of Radioactive Isotopes*, S. Shirley, Eds. New York, NY, USA: Wiley, 1986.

[3] S. Organizations, Multi-Agency Radiological Laboratory Analytical Protocols Manual (MARLAP). Cap 15 Quantification of Radionuclides. NUREG-1576 / EPA 402-B-04-001A / NTIS PB2004-105421, *United States Environmental Protection Agency et. al.*, Jul. 2004, http://www.epa.gov/radiation/marlap/manual.html

[4] W. John and G. Reischl, "Measurements of the filtration efficiencies of selected filter types," *Atmospher. Environ.*, vol. 12, pp. 2015–2019, 1978.

[5] E. Kitto and D. Anderson, "Correspondence. the use of whatman-41 filters for particle collection," *Atmospher. Environ.*, vol. 22, no. 11, pp. 2629–2630, 1988.

[6] Y. Miyamoto, K. Yasuda, and M. Magara, "Size distribution of radioactive particles collected at tokai, japan 6 days after the nuclear accident," *J. Environ. Radioact.*, vol. 132, pp. 1–7, 2014.

[7] E. Bondietti, J. Brantley, and C. Rangarajan, "Size distributions and growth of natural and chernobyl-derived submicron aerosols in tennessee," *J. Environ. Radioact.*, vol. 6, pp. 99–120, 1988.

[8] M. Naritomi, Y. Yoshida, and S. Fukuda, "Method for improving the collecting performance of iodine samplers under high relative humidity," *J. Nucl. Sci. Technol.*, vol. 10, no. 5, pp. 292–300, 1973.

[9] S. MacMullin, G. Giovanetti, M. Green, R. Henning, R. Holmes, K. Vorren, and J. Wilkerson, "Measurement of airborne fission products in Chapel Hill, NC, USA from the Fukushima Daiichi reactor accident," *J. Environ. Radioact.*, vol. 112, pp. 165–170, 2012.

[10] A. Chamberlain, *Radioactive Aerosols*, 1st Cambridge, U.K.: Cambridge Univ. Press, 1991.

[11] J. Ramsdell Jr., "Rascal 4.3. dispersion and deposition models," *Proc. 18th Annu. George Mason Univ. Conf. Atmospheric Transport and Dispersion Modelling*, 2014.

[12] G. Gilmore, *Practical Gamma-Ray Spectrometry*, Hoboken, NJ, USA: Wiley, 2008, http://books.google.es/books?id=mNHvAAAAMAAJ

[13] *Scintillation products, Tech. note, Brillance Scintillators Performance Summary,*, Saint Gobain Crystals Tech. Rep., 2009.